Stepwise and Concerted Pathways in Thermal and Photoinduced Electron−Transfer/Bond-Breaking Reactions

ARTICLE *in* THE JOURNAL OF PHYSICAL CHEMISTRY A · JULY 2000

Impact Factor: 2.69 · DOI: 10.1021/jp994426f

3 AUTHORS, INCLUDING:

Cyrille Costentin
Paris Diderot University
104 PUBLICATIONS **2,327** CITATIONS

SEE PROFILE

Marc Robert
Paris Diderot University
114 PUBLICATIONS **2,777** CITATIONS

SEE PROFILE

Stepwise and Concerted Pathways in Thermal and Photoinduced Electron-Transfer/Bond-Breaking Reactions

Cyrille Costentin, Marc Robert, and Jean-Michel Savéant*

Laboratoire d'Electrochimie Moléculaire, Unité Mixte de Recherche Université—CNRS No 7591, Université de Paris 7—Denis Diderot, 2 place Jussieu, 75251 Paris Cedex 05, France

Received: December 17, 1999; In Final Form: May 22, 2000

Bond cleavages triggered by electron transfer may follow a stepwise or a concerted mechanism. A proper description of the competition between the two reaction pathways requires a more detailed analysis of the reaction coordinate than usual. Such an analysis is presented for systems in which nuclear reorganization involves mostly the stretching of the cleaving bond and the reorganization of the solvent. It is first applied to thermal reactions such as electrochemical or homogeneous bond cleavages and then to photoinduced reactions. The quantum yields predicted for stepwise mechanisms are derived under conditions of practical interest and compared with the quantum yields predicted for concerted mechanisms. It is shown that quantum yields for stepwise mechanisms may approach unity and are not necessarily smaller than quantum yields for concerted mechanisms. The fragments resulting from bond cleavage may interact within the solvent cage where they are formed. The influence of such interactions on the dynamics of stepwise and concerted reactions is discussed.

Reactions in which single-electron transfer triggers the breaking of a chemical bond may follow two types of mechanisms, namely, a stepwise mechanism and a concerted electron-transfer mechanism, as pictured in Scheme 1. The dichotomy between these mechanisms and the passage from one mechanism to the other are currently under active investigation for thermal[1] as well as photoinduced[2] reactions.

With thermal reactions, a transition between the two reaction pathways has been observed within families of cleaving substrates upon varying their molecular properties[3] and also upon increasing the thermodynamic driving force offered to the reaction.[3c,4]

In the potential energy diagrams used so far to visualize the transition between concerted and stepwise pathways, the potential energy is plotted against a "reaction coordinate" which has not been clearly defined. To avoid any ambiguity in the analysis of such transitions, it is important to emphasize that the reaction coordinate is, in fact, not the same for the three reactions represented. This problem will be examined in the first of the following sections.

All photoinduced electron-transfer/bond-breaking reactions investigated so far exhibit quantum yields that are lower than unity. On the basis of the intuition that the quantum yield of a dissociative electron-transfer reaction should equal unity, it was inferred that the investigated reactions follow a stepwise mechanism, even if a concerted mechanism has been observed in the thermal reactions of the same cleaving substrates.[2c,5] It has, however, been recently shown that concerted mechanisms are not necessarily endowed with a unity quantum yield, as intuitively guessed.[6] The reason lies in the fact that the system partitions between fragmentation and back electron transfer in the funnel offered by the upper first-order potential energy surface, combining the ground state and fragment zero-order surfaces. We address, in the second section, the question of the quantum yields predicted in the case of a stepwise mechanism, so as to compare the result with the preceding evaluation of the quantum yields for concerted mechanisms.

Scheme 1

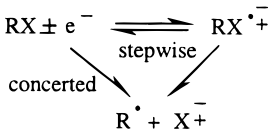

In the last section, we discuss how the existence of interactions between the product fragments within the solvent cage may affect the dynamics of the stepwise and the concerted pathways. There is, indeed, indirect experimental evidence that such attractive interactions, of the charge/dipole type, may exist in the gas phase after injection of an electron in alkyl halides.[7,8] Ab initio calculations give contrasting results, depending on the method used and approximations made.[9−11] It is usually assumed that these interactions vanish in polar solvents. One such case is the anionic state of CF_3Cl,[11] where the shallow minimum calculated in the gas phase disappears upon solvation, at least when a simple continuum solvation model is used. The attractive interaction existing in the gas phase may persist, even though weakened, in the caged product system in a polar solvent and, thus, influence the dynamics of the concerted and stepwise pathways.

Reaction Coordinates in Concerted and Stepwise Reactions

It is important to emphasize that the reaction coordinate is not the same for the three reactions represented in Scheme 1. With reactions in which the main nuclear reorganization factors involves solvent and bond cleavage, the length of the cleaving bond is a common ingredient for the three reactions but solvation reorganization requires a specific coordinate for each of them.

In the electrochemical case, starting with a molecule R−X, the dissociative electron-transfer reaction involves the solvent reorganization corresponding to the charging of the X portion of the molecule. For the formation of the ion radical, solvent

10.1021/jp994426f CCC: $19.00
Published on Web 07/21/2000

reorganization corresponds to the charging of the R portion of the molecule. For the cleavage of the ion radical, solvent reorganization corresponds to the transfer of the charge between two locations in the molecule, namely the R portion and the X portion.

Describing the dissociative electron-transfer step, $RX \pm e^- \Leftrightarrow R^\bullet + X^\mp$, involves determining the saddle point on the intersection of the two following free energy surfaces[12] (for the passage from potential energy surfaces to free energy surfaces see ref 13).

$$G_{RX\pm e^-} = G^0_{RX\pm e^-} + \lambda_{0,1}X_1^2 + DY_1^2 \quad (1)$$

$$G_{R^\bullet+X^\mp} = G^0_{R^\bullet+X^\pm} + \lambda_{0,1}(1-X_1)^2 + D(1-Y_1)^2 \quad (2)$$

where X_1 is a fictitious charge borne by the X portion of the molecule, serving as a solvation index for solvent reorganization around X, and $\lambda_{0,1}$ is the corresponding solvent reorganization energy.

$$Y_1 = 1 - \exp[-\beta(y - y_{RX})] \quad (3)$$

(with $\beta = \nu(2\pi^2\mu/D)^{1/2}$, y = bond length, y_{RX} = equilibrium value of y in RX, ν = frequency of the cleaving bond, and μ = reduced mass) is a variable representing the stretching of the cleaving bond. The coordinates of the saddle point are

$$X_1^{\neq} = Y_1^{\neq} = \frac{1}{2}\left(1 + \frac{G^0_{R^\bullet+X^\mp} - G^0_{RX\pm e^-}}{\lambda_{0,1} + D}\right) \quad (4)$$

$$\Delta G_1^{\neq} = \frac{\lambda_{0,1} + D}{4}\left(1 + \frac{G^0_{R^\bullet+X^\mp} - G^0_{RX\pm e^-}}{\lambda_{0,1} + D}\right)^2 \quad (5)$$

and the steepest descent pathway is given by the following two equations

$$0 \le X_1 \le X_1^{\neq}: \left(\frac{X_1}{X_1^{\neq}}\right)^{1/\lambda_{0,1}} = \left(\frac{Y_1}{Y_1^{\neq}}\right)^{1/D} \quad (6)$$

$$X_1^{\neq} \le X_1 \le 1: \left(\frac{1-X_1}{1-X_1^{\neq}}\right)^{1/\lambda_{0,1}} = \left(\frac{1-Y_1}{1-Y_1^{\neq}}\right)^{1/D} \quad (7)$$

An example is given in Figure 1. The dotted line in Figure 1a shows the projection of the steepest descent pathway on the $X_1 - Y_1$ plane, while the full line is the projection of the intersection of the two surfaces 1 and 2. A three-dimensional representation of the steepest descent pathway is given in Figure 1b. We may combine X_1 and Y_1 so as to define a reaction coordinate, Z_1, according to eq 8, where the normalization is adjusted so as to obtain $Z_1 = 1$ for the product state, that is, for $X_1 = Y_1 = 1$.

$$Z_1 = \frac{\int_0^{X_1}\sqrt{1 + \left(\frac{dY_1}{dX_1}\right)^2}\,d\eta}{\int_0^1\sqrt{1 + \left(\frac{dY_1}{dX_1}\right)^2}\,d\eta} \quad (8)$$

Thus, when $0 \le X_1 \le X_1^{\neq}$

$$Z_1 = X_1^{\neq}\frac{\int_0^{X_1/X_1^{\neq}}\sqrt{1 + \left(\frac{D}{\lambda_{0,1}}\eta^{D/\lambda_{0,1}-1}\right)^2}\,d\eta}{\int_0^1\sqrt{1 + \left(\frac{D}{\lambda_{0,1}}\eta^{D/\lambda_{0,1}-1}\right)^2}\,d\eta} \quad (9)$$

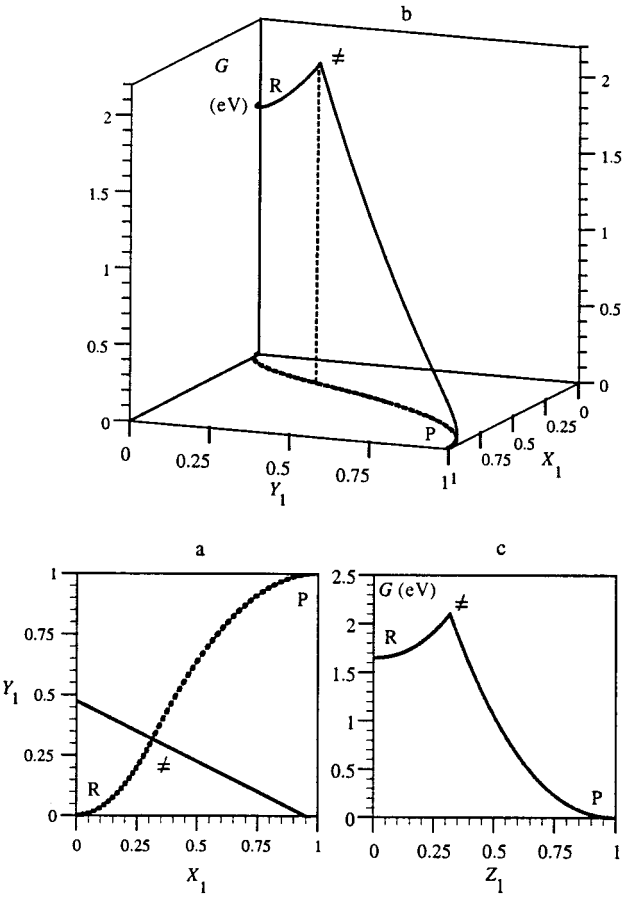

Figure 1. $RX \pm e^- \Leftrightarrow R^\bullet + X^\mp$. In electronvolts, $D = 3$, $\lambda_{0,1} = 1.5$, $G^0_{RX\pm e^-} = 1.65$, $G^0_{R^\bullet+X^\mp} = 0$. (a) Full line: projection of the intersection of the two surfaces 1 and 2, dotted line: projection of the steepest descent pathway. (b) Steepest descent reaction pathway. (c) Steepest descent reaction profile as a function of the reaction coordinate Z_1. R: $RX \pm e^-$, P: $R^\bullet + X^\mp$.

When $X_1^{\neq} \le X_1 \le 1$:

$$Z_1 = 1 - (1-X_1^{\neq})\frac{\int_0^{(1-X_1)/(1-X_1^{\neq})}\sqrt{1 + \left(\frac{D}{\lambda_{0,1}}\eta^{D/\lambda_{0,1}-1}\right)^2}\,d\eta}{\int_0^1\sqrt{1 + \left(\frac{D}{\lambda_{0,1}}\eta^{D/\lambda_{0,1}-1}\right)^2}\,d\eta} \quad (10)$$

The resulting reaction profile is shown in Figure 1c.

The same type of analysis can be repeated for the two other reactions using appropriate free energy surfaces.[14]

For $RX \pm e^- \Leftrightarrow RX^{\bullet\mp}$

$$G_{RX\pm e^-} = G^0_{RX\pm e^-} + D\{1 - \exp[-\beta(y - y_{RX})]\}^2 + \lambda_{0,2}X_2^2 \quad (11)$$

$$G_{RX^{\bullet\mp}} = G^0_{RX^{\bullet\mp}} + D'\{1 - \exp[-\beta(y - y_{RX^{\bullet\mp}})]\}^2 + \lambda_{0,2}(1 - X_2)^2 \quad (12)$$

after introduction of another coordinate, X_2, depicting the solvent reorganization around the R portion of the molecule and of the corresponding solvent reorganization energy $\lambda_{0,2}$. The effect of bond stretching is represented by a Morse curve (D' being the homolytic bond dissociation energy of $RX^{\bullet\mp}$), which has the same repulsive part as the RX Morse curve.[14] This condition implies that the two equilibrium values of the bond length are related by eq 13

$$y_{RX^{\bullet\mp}} - y_{RX} = \frac{1}{\beta}\ln\left(\frac{\sqrt{D}}{\sqrt{D'}}\right) \quad (13)$$

We may, thus, introduce another stretching coordinate, Y_2, defined as

$$Y_2 = \frac{\sqrt{D}}{\sqrt{D} - \sqrt{D'}} Y_1 \quad (14)$$

Equations 11 and 12 thus become

$$G_{RX\pm e^-} = G^0_{RX\pm e^-} + (\sqrt{D} - \sqrt{D'})^2 Y_2^2 + \lambda_{0,2} X_2^2 \quad (15)$$

$$G_{RX^{\bullet\mp}} = G^0_{RX^{\bullet\mp}} + (\sqrt{D} - \sqrt{D'})^2 (1 - Y_2)^2 + \lambda_{0,2}(1 - X_2)^2 \quad (16)$$

and

$$X_2^{\neq} = Y_2^{\neq} = \frac{1}{2}\left[1 + \frac{G^0_{RX^{\bullet\mp}} - G^0_{RX\pm e^-}}{\lambda_{0,2} + (\sqrt{D} - \sqrt{D'})^2}\right] \quad (17)$$

$$\Delta G_2^{\neq} = \frac{\lambda_{0,2} + (\sqrt{D} - \sqrt{D'})^2}{4}\left[1 + \frac{G^0_{RX^{\bullet\mp}} - G^0_{RX\pm e^-}}{\lambda_{0,2} + (\sqrt{D} - \sqrt{D'})^2}\right]^2 \quad (18)$$

Finally, the reaction coordinate, Z_2, is obtained by application of equations that are identical to eqs 9 and 10, in which X_2, $\lambda_{0,2}$, and $(\sqrt{D} - \sqrt{D'})^2$ replace X_1, $\lambda_{0,1}$, and D, respectively.

For $RX^{\bullet\mp} \leftrightarrow R^{\bullet} + X^{\mp}$,

$$G_{RX^{\bullet\mp}} = G^0_{RX^{\bullet\mp}} + D'\{1 - \exp[-\beta(y - y_{RX^{\bullet\mp}})]\}^2 + \lambda_{0,3} X_3^2 \quad (19)$$

$$G_{R^{\bullet}+X^{\mp}} = G^0_{R^{\bullet}+X^{\mp}} + D\{\exp[-\beta(y - y_{RX})]\}^2 + \lambda_{0,3}(1 - X_3)^2 \quad (20)$$

after introduction of another coordinate, X_3, depicting the reorganization of the solvent upon shifting the charge from the R to the X portion of the molecule and of the corresponding solvent reorganization energy $\lambda_{0,3}$. The effect of bond stretching is represented by a Morse curve for $RX^{\bullet\mp}$ and by a purely repulsive Morse curve for the fragments.[14] We may introduce a new stretching coordinate, Y_3, defined as

$$Y_3 = 1 - \exp[-\beta(y - y_{RX^{\bullet\mp}})] = 1 - \frac{\sqrt{D}}{\sqrt{D'}}(1 - Y_1) \quad (21)$$

Equations 19 and 20 thus become

$$G_{RX^{\bullet\mp}} = G^0_{RX^{\bullet\mp}} + D' Y_3^2 + \lambda_{0,3} X_3^2 \quad (22)$$

$$G_{R^{\bullet}+X^{\mp}} = G^0_{R^{\bullet}+X^{\mp}} + D'(1 - Y_3)^2 + \lambda_{0,3}(1 - X_3)^2 \quad (23)$$

and

$$X_3^{\neq} = Y_3^{\neq} = \frac{1}{2}\left[1 + \frac{G^0_{R^{\bullet}+X^{\mp}} - G^0_{RX^{\bullet\mp}}}{\lambda_{0,3} + D'}\right] \quad (24)$$

$$\Delta G_3^{\neq} = \frac{\lambda_{0,3} + D'}{4}\left[1 + \frac{G^0_{R^{\bullet}+X^{\mp}} - G^0_{RX^{\bullet\mp}}}{\lambda_{0,3} + D'}\right]^2 \quad (25)$$

Finally, the reaction coordinate, Z_3, is obtained by application of equations that are identical to eqs 9 and 10, in which X_3, $\lambda_{0,3}$, and D' replace X_1, $\lambda_{0,1}$, and D, respectively.

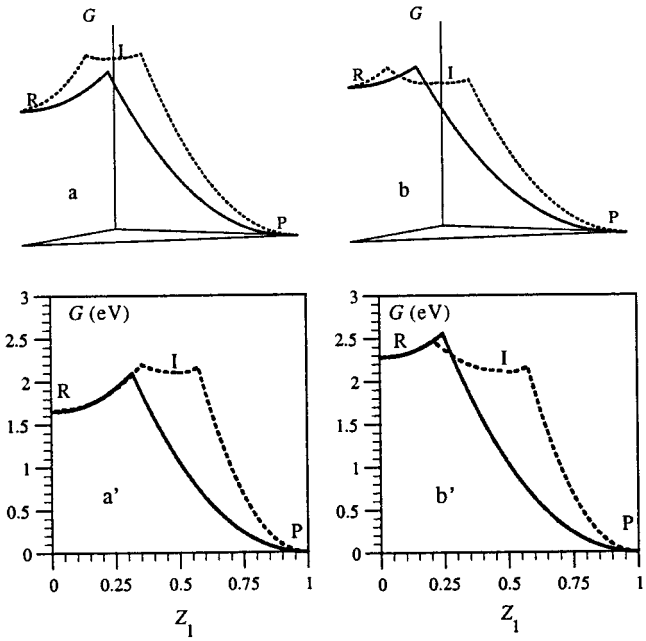

Figure 2. 3-dimensional (a, b) and 2-dimensional (a′, b′) representations of the concerted (full line) and stepwise (dotted lines) reaction pathways. $RX \pm e^- \leftrightarrow R^{\bullet} + X^{\mp}$: $D = 3$ eV, $\lambda_{0,1} = 1.5$ eV, $G^0_{RX} = 1.65$ eV (left-hand diagrams), 2.28 eV (right-hand diagrams). $RX \pm e^- \leftrightarrow RX^{\bullet\mp}$: $(\sqrt{D} - \sqrt{D'})^2 = 0.1$ eV, $\lambda_{0,2} = 1$ eV, $G^0_{RX^{\bullet\mp}} = 2.1$ eV. $RX^{\bullet\mp} \leftrightarrow R^{\bullet} + X^{\mp}$: $D' = 2$ eV, $\lambda_{0,3} = 1$ eV, $G^0_{R^{\bullet}+X^{\mp}} = 0$. R: reactants ($RX \pm e^-$), I: intermediate ($RX^{\bullet\mp}$), P: products ($R^{\bullet} + X^{\mp}$).

It follows that a proper description of the stepwise and concerted reaction pathways requires a three-dimensional representation, as illustrated by Figures 2a and b.

The example chosen in Figure 2 corresponds to the passage from a concerted to a stepwise mechanism, as observed by means of cyclic voltammetry upon increasing the scan rate and/or decreasing the temperature. At the peak, the free energy of activation is given by eq 26[3a,b]

$$\Delta G^{\ddagger} = \frac{RT}{F}\left[\ln\left(Z^{el}\sqrt{\frac{RT}{\alpha F \upsilon D_i}}\right) - 0.78\right] \quad (26)$$

and $Z^{el} = \sqrt{RT/2\pi M}$ (where M is the molar mass) is the electrochemical collision frequency, υ is the scan rate, and D_i is the diffusion coefficient. Taking typical values ($Z^{el} = 4 \times 10^3$ cm s^{-1} and $D_i = 10^{-5}$ cm^2 s^{-1}) leads to a bracketing of the free energy of activation at the peak between 0.385 eV (for $\upsilon = 0.1$ V/s, $T = 301$ K) and 0.185 eV (for $\upsilon = 10^3$ V/s, $T = 253$ K), from which the values of the standard free energies of reaction used in Figure 2 were derived.

Parts a′ and b′ of Figure 2 represent the projection of the reaction pathways on the same plane, namely the front plane, in which the dissociative electron-transfer step is represented. This two-dimensional representation is easier to decipher than the three-dimensional representation for determining the preferred pathway. They may, however, be misleading if it is not borne in mind that, in the two-dimensional representation, the crossings between the three curves should not be considered as actual crossings of reaction pathways.

Quantum Yields of Stepwise Reactions

The reaction pathways can be obtained from the following free energy surfaces, according to the procedure depicted in the

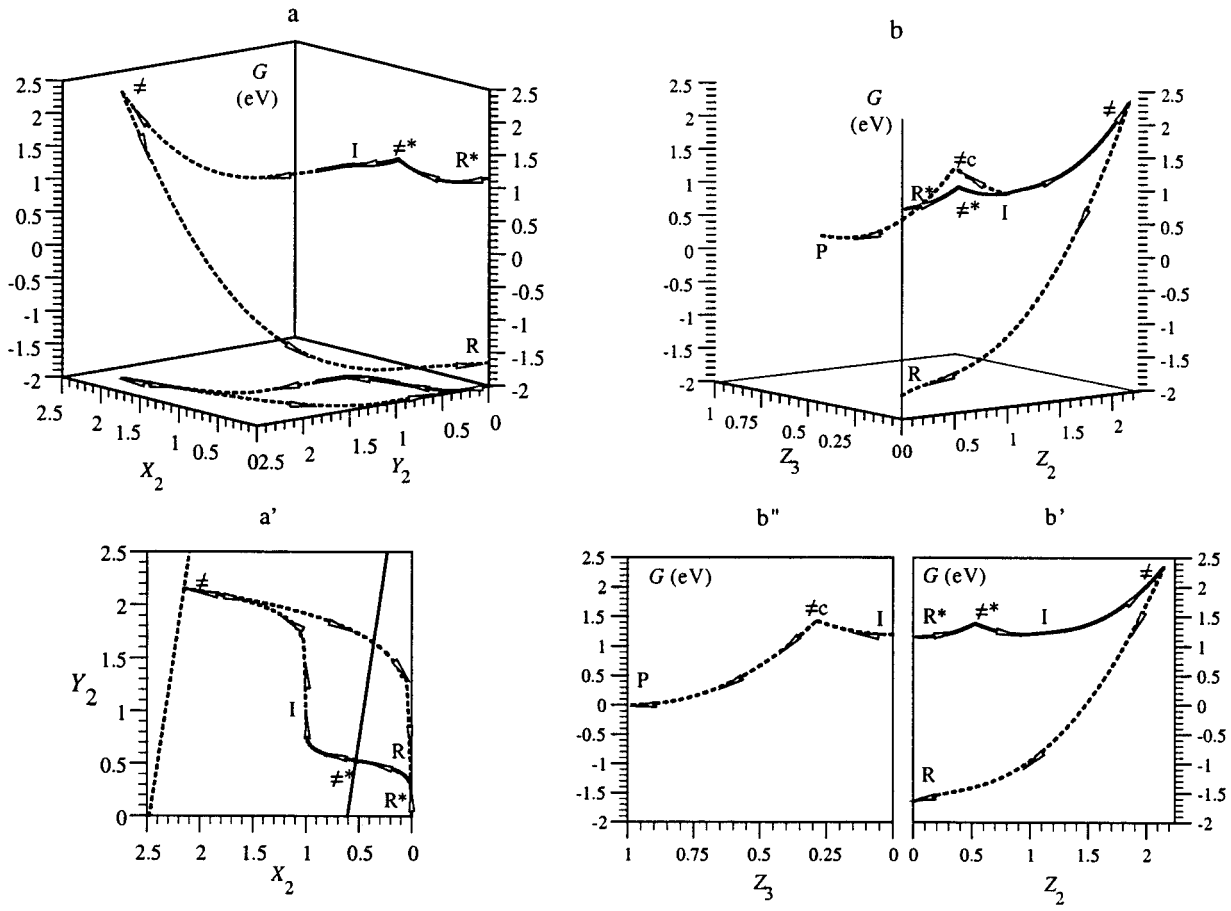

Figure 3. Reaction pathway for a photoinduced reaction following a stepwise mechanism in which the electron transfer is in the inverted region. In eV, $G^0_{D^*+RX} = 1.15$, $G^0_{D+RX} = -1.65$, $G^0_{D^{\bullet+}+RX^{\bullet-}} = 1.2$, $G^0_{D^{\bullet+}+R^{\bullet}+X^-} = 0$, $(\sqrt{D} - \sqrt{D'})^2 = 0.1$, $D' = 1.8$, $\lambda_{0,2} = 0.75$, $\lambda_{0,3} = 1$. R*: D* + RX, R: D + RX, I: $D^{\bullet+} + RX^{\bullet-}$, P: $D^{\bullet+} + R^{\bullet} + X^-$. ≠*, ≠, ≠c, transition states of the photoinduced electron transfer, back electron transfer, and cleavage, respectively.

preceding section. For simplicity of symbols, we treat only the case of a reductive cleavage. Transposition to an oxidative process is straightforward.

For the photoinduced electron-transfer step and for the back electron-transfer step

$$G^*_{RX+D^*} = G^{*,0}_{RX+D^*} + (\sqrt{D} - \sqrt{D'})^2 Y_2^2 + \lambda_{0,2} X_2^2 \quad (27)$$

$$G_{RX+D} = G^0_{RX+D} + (\sqrt{D} - \sqrt{D'})^2 Y_2^2 + \lambda_{0,2} X_2^2 \quad (28)$$

$$G_{RX^{\bullet-}+D^{\bullet+}} = G^0_{RX^{\bullet-}+D^{\bullet+}} + (\sqrt{D} - \sqrt{D'})^2 (1 - Y_2)^2 + \lambda_{0,2}(1 - X_2)^2 \quad (29)$$

For the cleavage step

$$G_{RX^{\bullet-}+D^{\bullet+}} = G^0_{RX^{\bullet-}+D^{\bullet+}} + D' Y_3^2 + \lambda_{0,3} X_3^2 \quad (30)$$

$$G_{R^{\bullet}+X^-+D^{\bullet+}} = G^0_{R^{\bullet}+X^-+D^{\bullet+}} + D'(1 - Y_3)^2 + \lambda_{0,3}(1 - X_3)^2 \quad (31)$$

It is convenient to distinguish the two situations according to whether the electron-transfer step of the stepwise mechanism lies in the normal or in the inverted region.

Back Electron Transfer in the Inverted Region. Past the transition state of the photoinduced reaction, the point representing the system reaches the ion-radical intermediate, I, before crossing the potential energy surface of the ground state, as illustrated in Figure 3. The intermediate I may then competitively undergo back electron transfer, going over the inverted region barrier (rate constant k_{-act}), and cleavage (rate constant k_c) according to Scheme 2.

Scheme 2

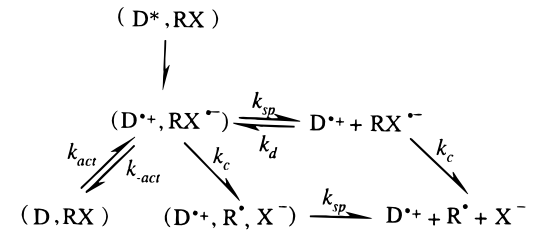

Figure 3a shows the photoinduced and the back electron-transfer pathways as a function of the two coordinates, X_2 and Y_2, representing the solvent reorganization and bond stretching, respectively. Figure 3a′ shows the projection of the three-dimensional reaction pathways on the X_2/Y_2 plane. The straight lines are the projections of the intersection between the excited reactant state surface and the intermediate surface (full line) and of the intersection between the ground reactant state surface and the intermediate surface (dotted line). Although the photoinduced and back electron-transfer pathways have different projections, the element of arc length, dZ_2, is the same function of $\lambda_{0,2}$ and $(\sqrt{D} - \sqrt{D'})^2$ in both cases. We may, thus, use the same reaction coordinate, Z_2, as defined in the preceding section for the two pathways, bearing in mind that their traces on the X_2/Y_2 plane are not the same. For the cleavage reaction, we introduce the reaction coordinate Z_3, as defined in the preceding section. Using these two coordinates, parts b, b′, and b″ of Figure

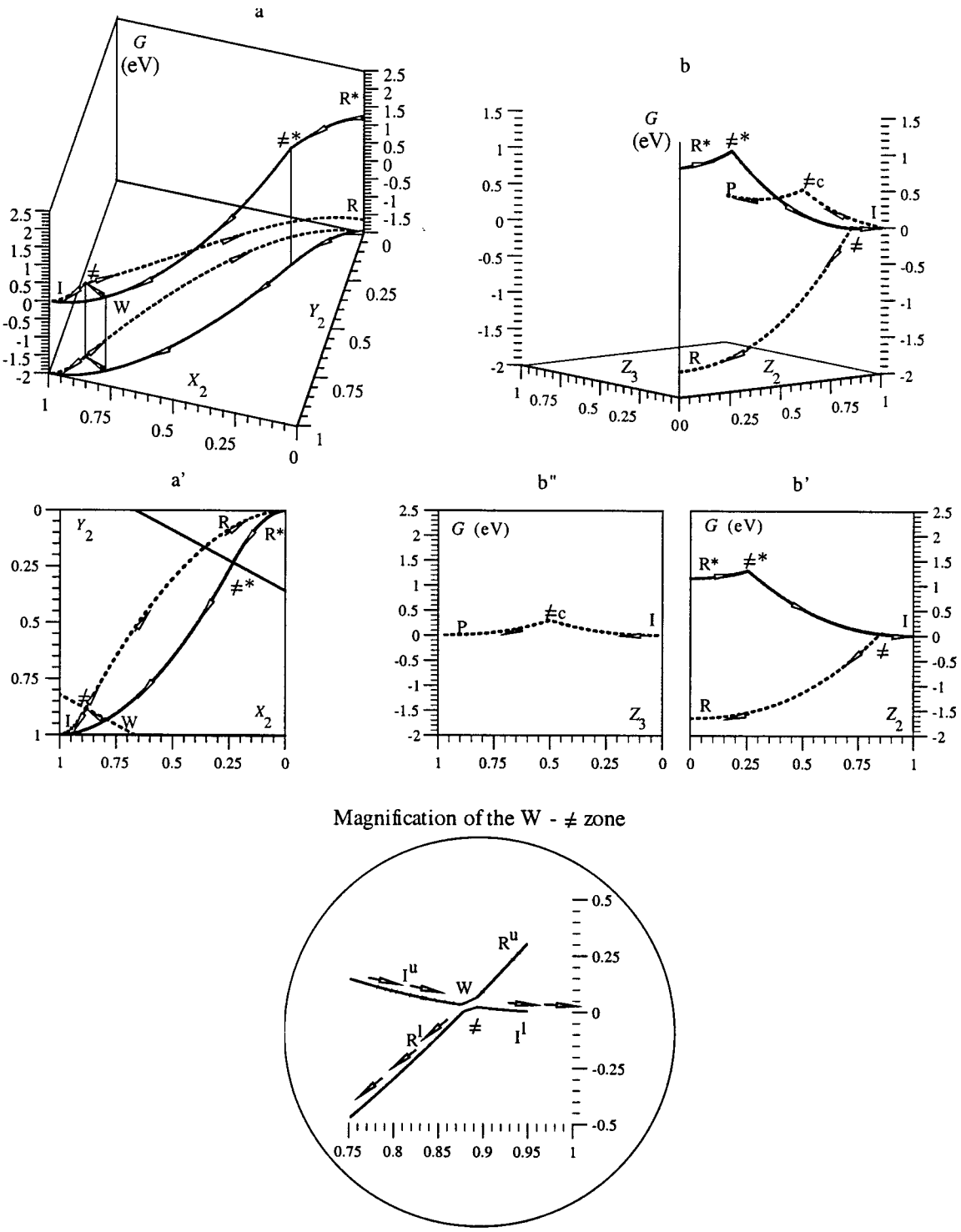

Figure 4. Reaction pathway for a photoinduced reaction following a stepwise mechanism in which the electron transfer is in the normal region. In eV, $G^0_{D^*+RX} = 1.15$, $G^0_{D+RX} = -1.65$, $G^0_{D^{\bullet+}+RX^{\bullet-}} = 0$, $G^0_{D^{\bullet+}+R^{\bullet}+X^-} = 0$, $(\sqrt{D} - \sqrt{D'})^2 = 1.4$, $D' = 0.22$, $\lambda_{0,2} = 0.75$, $\lambda_{0,3} = 1$. R*: $D^* + RX$, R: $D + RX$, I: $D^{\bullet+} + RX^{\bullet-}$, P: $D^{\bullet+} + R^{\bullet} + X^-$.

3 give a representation of the whole stepwise mechanism involving photoinduced electron transfer, back electron transfer, and cleavage of the intermediate.

Turning back to Scheme 2, we may assume for simplicity that the rate constants for the diffusion of the anion radical and of the fragments from the solvent cage are the same (k_{sp}), and so are the cleavage rate constants of the anion radical within and outside the solvent cage (there is no theoretical difficulty in extending the analysis to cases where these simplifications do not apply). The most interesting case, for the purpose of the present discussion, is when the cleavage rate constant is large enough to prevent the diffusion of the cation and anion radicals, one toward the other. The quantum yield for the photoinduced reductive cleavage is, thus, given by eq 32 (in practice, the electron transfer from the ground-state donor is so uphill a reaction that k_{act} is negligible),

$$\Phi = \frac{k_{sp} + k_c}{k_{sp} + k_c + k_{-act}} \tag{32}$$

Scheme 3

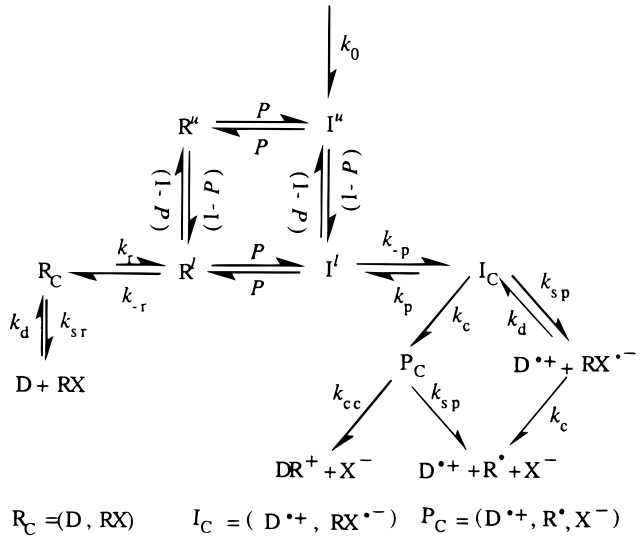

that is, by a simple extension of the expression of the quantum yield for an outer sphere photoinduced electron transfer in the inverted region.[15]

It appears that very high quantum yields approaching unity may well be obtained by combining a fast cleavage with a relatively high inverted region barrier. This is clearly the case with the values of the parameters used for the illustrative system shown in Figure 3.

Back Electron Transfer in the Normal Region. In this case, past the transition state of the photoinduced electron transfer, ≠*, at the intersection of the R* and I surfaces, the system reaches the intersection between the later surface and the ground state (R) surface in a point W (Figure 4a and its projection on the X_2-Y_2 plane, 4a′) before reaching the minimum corresponding to I. The transition state of the ground-state electron-transfer reaction, ≠, is also located on this intersection. The system, thus, bounces down from W to ≠, while passing from the upper to the lower first-order surface, in a fashion similar to the previously described case of a dissociative electron-transfer reaction,[6] thus, partitioning between back electron transfer and formation of the intermediate as a function of the magnitude of the electronic coupling matrix element between the I and R states, *H*. The intermediate then competitively undergoes back electron transfer and cleavage. Although the photoinduced and back electron-transfer pathways have different projections, the element of arc length, dZ_2, is the same function of $\lambda_{0,2}$ and $(\sqrt{D} - \sqrt{D'})^2$ in both cases. We may, thus, use the same reaction coordinate, Z_2, as defined in the preceding section, for the two pathways, bearing in mind that their traces on the X_2/Y_2 plane are not the same. For the cleavage reaction, we introduce the reaction coordinate Z_3, as defined in the preceding section. Using these two coordinates, parts b, b′, and b″ of Figure 4 give a representation of the whole stepwise mechanism involving photoinduced electron transfer, back electron transfer, and cleavage of the intermediate. We see on these representations as well as in Scheme 3, which summarizes all the reactions involved, that back electron transfer interferes twice: once, at the intersection between the zero-order I and R surfaces and, a second time, from the intermediate through back crossing of the ground-state electron-transfer barrier. *P* is the probability that the system remains on the first-order potential energy surfaces formed by a combination of the zero-order potential surfaces near their intersection. In the framework of the Landau−Zener model, *P* is related to *H* by means of eq 33.

$$P = 1 - \exp\left\{-\frac{\pi^{3/2}H^2}{h\nu(RT)^{1/2}[(\sqrt{D} - \sqrt{D'})^2 + \lambda_{0,2}]^{1/2}}\right\} \quad (33)$$

(where ν is the effective vibration frequency of the reactants).[16] Introducing the ratios, κ, of the rate constants k and of the frequency ν,

$$\frac{d[X^-]}{\nu\, dt} = (\kappa_{sp} + \kappa_{cc})[P_C] + \kappa_c[RX^{\bullet-}] \quad (34)$$

Since,

$$[RX^{\bullet-}] = \frac{\kappa_{sp}}{\kappa_d[D^{\bullet+}] + \kappa_c}[I_C] \quad (35)$$

and

$$(\kappa_{sp} + \kappa_{cc})[P_C] = \kappa_c[I_C] \quad (36)$$

$$\frac{d[X^-]}{\nu\, dt} = \kappa_c\left(1 + \frac{\kappa_{sp}}{\kappa_d[D^{\bullet+}] + \kappa_c}\right)[I_C] \quad (37)$$

Thus, if we consider only the cases where the cleavage is fast enough to overcome the diffusion of $RX^{\bullet-}$ toward $D^{\bullet+}$,

$$\frac{d[X^-]}{\nu\, dt} = (\kappa_{sp} + \kappa_c)[I_C] \quad (38)$$

$$\frac{d[D]}{\nu\, dt} = \frac{d[RX]}{\nu\, dt} = \kappa_{sr}[R_C] - \kappa_d[D][RX] \quad (39)$$

$$\kappa_p[I^l] - (\kappa_p + \kappa_{sp} + \kappa_c)[I_C] = 0 \quad (40)$$

$$\kappa_r[R^l] + \kappa_d[D][RX] - (\kappa_r + k_{sr})[R_C] = 0 \quad (41)$$

$$\kappa_p[I_C] + P[R^l] + (1 - P)[I^u] - (1 + \kappa_{-p})[I^l] = 0 \quad (42)$$

$$\kappa_r[R_C] + P[I^l] + (1 - P)[R^u] - (1 + \kappa_{-r})[R^l] = 0 \quad (43)$$

$$\kappa_0 + (1 - P)[I^l] + P[R^u] - [I^u] = 0 \quad (44)$$

$$(1 - P)[R^l] + P[I^u] - [R^u] = 0 \quad (45)$$

The rest of the resolution is exactly the same as that for dissociative electron transfer,[6] replacing κ_{cc} with κ_c and *P* with I. Therefore,

$$\Phi = \frac{1}{(1 + P)\left(1 + \frac{2P}{1 + P}\,\frac{k_{-act}}{k_{sp} + k_c}\right)} \quad (46)$$

with *P* being related to the electronic coupling matrix element by means of eq 33. Another demonstration of eq 46, taking more rigorously into account the stretching and solvent reorganization coordinates, may be obtained by a straightforward transposition of the case of dissociative electron transfer.[6]

In total, the situation is less favorable in terms of quantum yields than in the preceding case. Indeed, even if the cleavage rate constant is large enough for overrunning back electron transfer from the ion pair ($k_c \gg k_{-act}$), the maximal value of

the quantum yield is $1/(1 + P)$, which would reach unity only in the unlikely case where the ground-state electron transfer would be entirely nonadiabatic ($H = 0$).

Influence of Interactions between the Caged Product Fragments. We first examine the influence of these interactions on the *dynamics of dissociative electron transfers*. As shown by recent quantum mechanical calculations combined with a cyclic voltammetric study of the reduction of carbon tetrachloride,[17] the interaction between the two fragments in the gas phase may be modeled by a Morse curve, with a shallow minimum, even if the nature of the interaction is more of a charge−dipole (and induced dipole) type rather than that of a covalent bond. It also appears that the repulsive part of the fragments' Morse curve is almost identical to the repulsive part of the Morse curve depicting the homolytic dissociation of the starting RX molecule. Assuming that this behavior is general, the reactant and product free energies may be expressed by eqs 47 and 48, respectively.

$$G_{RX\pm e^-} = G^0_{RX\pm e^-} + D\{1 - \exp[-\beta(y - y_R)]\}^2 + \lambda_{0,1}X_1^2 \quad (47)$$

$$G_{(R^\bullet,X^\mp)} = G^0_{(R^\bullet,X^\mp)} - \Delta G^0_{sp} + D_P\{1 - \exp[-\beta(y - y_P)]\}^2 + \lambda_{0,1}(1 - X_1)^2 \quad (48)$$

y_R and y_P are the values of the R···X distances in the reactant and product systems, respectively. The interaction energy is involved in the Morse function and also in the difference between the standard free energies of the separated and the caged fragments, $\Delta G^0_{sp} = D_P - T\Delta S_{sp}{}^0$. The assumption that the repulsive terms in the two Morse curves are approximately the same leads to eq 49, relating the difference in the equilibrium distances to the ratio of the dissociation energies.

$$y_P = y_R + \frac{1}{2\beta}\ln\left(\frac{D}{D_P}\right) \quad (49)$$

Equation 49 indicates that a shallow minimum ($D_P \ll D$) corresponds to a loose cluster ($y_P \gg y_R$) and vice versa.

The governing equations are, thus, the same as those for the $RX \pm e^- \leftrightarrow RX^{\bullet\mp}$ reaction discussed in the first section, although the physical situation is not the same, in the sense that the species that is formed (i.e., the caged product fragments) is not a strongly unstable species toward bond breaking. It follows that the dynamics of this "sticky" dissociative electron transfer may be depicted by the following set of equations:

$$G_{RX\pm e^-} = G^0_{RX\pm e^-} + (\sqrt{D} - \sqrt{D_P})^2 Y'^2_1 + \lambda_{0,1}X_1^2 \quad (50)$$

$$G_{(R^\bullet,X^\mp)} = G^0_{(R^\bullet,X^\mp)} + (\sqrt{D} - \sqrt{D_P})^2(1 - Y'_1)^2 + \lambda_{0,1}(1 - X_1)^2 \quad (51)$$

where $(R^\bullet,X^\mp)$ represents the interacting caged fragments with

$$Y'_1 = \frac{\sqrt{D}}{\sqrt{D} - \sqrt{D_P}}Y_1 \quad (52)$$

and

$$X_1^{\neq} = Y'^{\neq}_1 = \frac{1}{2}\left[1 + \frac{G^0_{(R^\bullet,X^\mp)} - G^0_{RX\pm e^-}}{\lambda_{0,1} + (\sqrt{D} - \sqrt{D_P})^2}\right] \quad (53)$$

$$\Delta G'^{\neq}_1 = \frac{\lambda_{0,1} + (\sqrt{D} - \sqrt{D_P})^2}{4}\left[1 + \frac{G^0_{(R^\bullet,X^\mp)} - G^0_{RX\pm e^-}}{\lambda_{0,1} + (\sqrt{D} - \sqrt{D_P})^2}\right]^2 \quad (54)$$

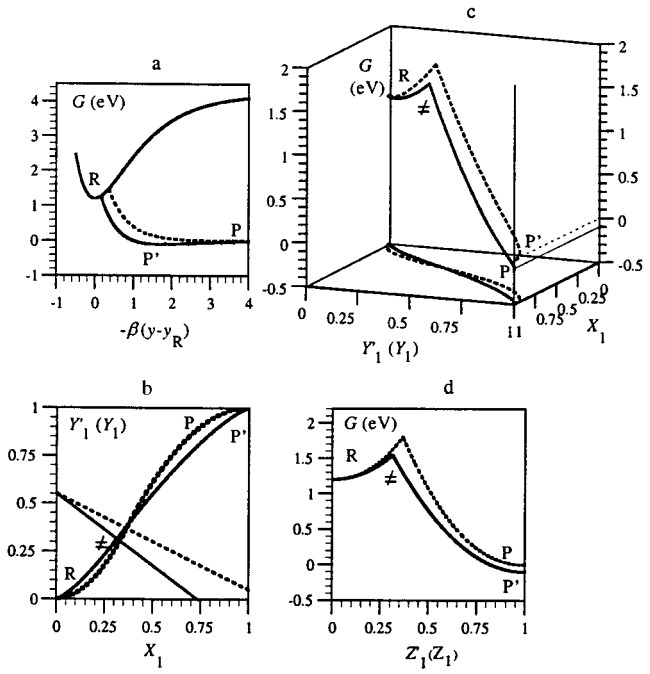

Figure 5. Influence of a small interaction between caged fragments. Full lines: $RX \pm e^- \leftrightarrow (R^\bullet,X^\mp)$. Dotted lines: $RX \pm e^- \leftrightarrow R^\bullet + X^\mp$. In eV, $D = 3$, $\lambda_{0,1} = 1.5$, $D_P = 0.1$, $G^0_{RX\pm e^-} = 1.65$, $G^0_{R^\bullet+X^\mp} = 0$, $G^0_{(R^\bullet,X^\mp)} = -0.1$. (a) Morse curves for the reactant, interacting fragments and separated fragments. (b) Projection of the reaction pathways on the $X_1 - Y'_1$ plane. (c) Reaction profiles as a function of the reaction coordinate Z'_1 or Z_1. R: $RX \pm e^-$, P: $R^\bullet + X^\mp$, P': $(R^\bullet,X^\mp)$. (d) Steepest descent reaction profile as a function of the reaction coordinate Z'_1 or Z_1.

Figure 5 illustrates, with a typical example, the effect of a small interaction between the caged fragments by comparison with a purely dissociative electron-transfer reaction.

It is noteworthy that a small value of D_P produces rather strong effects on the activation barrier.[18] The reason for such a large effect is that it is not merely a work term effect but that it has a significant effect on the intrinsic barrier in which D is replaced by $(\sqrt{D} - \sqrt{D_P})^2$. For example, if D_P is 4% of D, a decrease of ~20% of the intrinsic barrier ensues.

The electrochemical reduction of carbon tetrachloride offers an example where the interaction between fragments is rather strong in the gas phase (~0.4 eV), as revealed by ab initio calculations, and appears to persist in a polar solvent, albeit reduced to ~0.06 eV.

Other recent observations concerning substituted benzyl halides may also be rationalized within the same framework. Whereas the electrochemical reduction of 4-nitrobenzyl bromide in DMF is clearly a stepwise reaction, a concerted mechanism is observed with unsubstituted benzyl and 4-cyanobenzyl bromides.[3a] The cyclic voltammetric peak potential of 4-cyanobenzyl bromide is significantly more positive than the cyclic voltammetric peak potential of benzyl bromide (by 250 mV at a scan rate of 0.1 V/s). It was inferred from these observations that the bond dissociation energy increases by 0.15 eV from the first to the second compound, in line with previous photoacoustic work[19a] in which the substituent effect was regarded as concerning the starting molecule rather than the radical. However, further measurements using the same technique did not detect any substituent effect and the same conclusion was also reached in the gas phase by a low-pressure pyrolysis technique.[19b] Recent quantum chemical estimations[19c] concluded that there is a small sub-

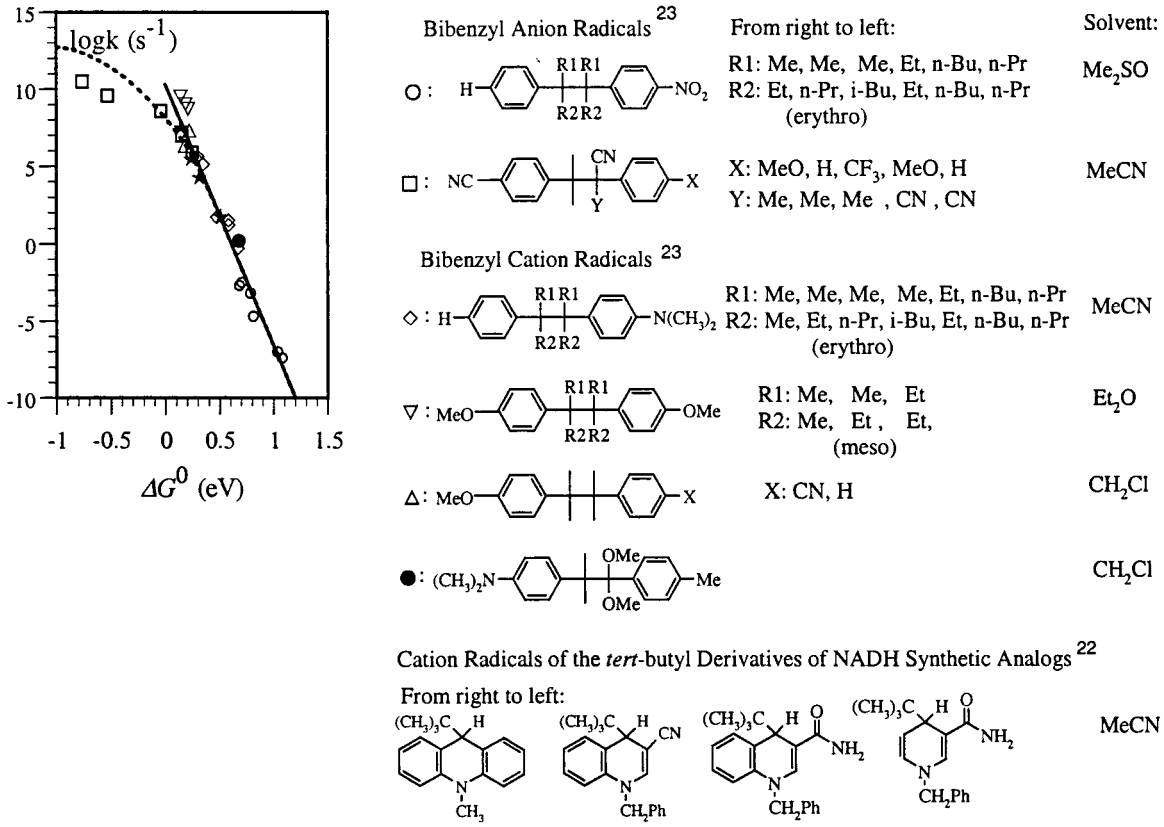

Figure 6. Variation of the rate constant with the driving force in the homolytic cleavage of various types of anion and cation radicals. The open symbols refer to bi-benzyl derivatives, and the stars refer to cation radicals of the *tert*-butyl derivatives of synthetic analogues of NADH.

stituent effect, namely, 0.07 eV, that is, about half of the value derived from electrochemical experiments upon application of the classical dissociative electron-transfer theory. These observations may well be interpreted by a small attractive interaction in the caged product fragments that would be larger in the presence rather than in the absence of the cyano-substituent because of its electron-withdrawing character. An even larger similar effect is observed with phenacyl chloride and bromide, as expected from the electron-withdrawing effect of the carbonyl group. The apparent BDEs derived from cyclic voltammetry are 2.05 and 2.35 eV for the bromide and chloride, respectively,[3d] whereas the values found by low pressure pyrolysis are 2.75 and 3.13 eV, respectively.[19d] The two sets of results may be reconciled after introduction of an interaction energy of 51 and 56 meV for the bromide and chloride, respectively.

The kinetics of the reduction of a series of organic disulfides[20] seems to fit this framework. The values found for the electrochemical standard rate constant for diphenyl disulfide and a series of 4,4′-substituted derivatives indicate a large intramolecular reorganization energy for the unsubstituted disulfide and for electron donating substituents, close to the predictions of the classical dissociative electron-transfer model. The standard rate constant rapidly increases upon introduction of more and more electron-withdrawing substituents, ending up, in the case of the nitro-substituents, with values that are indicative of solvent reorganization with little intramolecular reorganization. These trends indicate that the interaction between the caged fragments is negligible in the unsubstituted derivative and in the case of electron-donating substituents. Because the positive charge on the functional sulfur augments, the interaction between the fragments increases with the electron-withdrawing character of the substituent. With the nitro-derivative, it has become a true

Scheme 4[a]

$$RX^{\bullet\mp} \underset{k_-^{act}}{\overset{k_+^{act}}{\rightleftharpoons}} \left(R^{\bullet}, X^{\mp}\right) \underset{k_{dif}}{\overset{k'_{dif}}{\rightleftharpoons}} R^{\bullet} + X^{\mp}$$

[a] k_+^{act}, k_-^{act}: forward and reverse activation controlled rate constants. $K = k_+^{act}/k_-^{act}$ k'_{dif}: rate constant for the diffusion of the fragments out of the solvent cage, k_{dif}: bimolecular diffusion-limited rate constant.

bond. Because the unpaired and the negative charge are located on the same nitrophenyl part of the molecule, the dissociation of the anion radical is of the homolytic type.

It is also interesting to note that the above model applies to electron transfers leading to an ion radical that dissociates homolytically in an endothermic manner with a negligible barrier for the back coupling. Although all homolytically dissociating ion radicals do not behave in this manner,[21] several examples can be found where, in the framework of Scheme 4 and of eqs 55 and 56, the observed kinetics is governed by

$$k_+ = \frac{k'_{dif} k_+^{act}}{k'_{dif} + k_-^{act}} \tag{55}$$

$$k_- = \frac{k_{dif} k_-^{act}}{k'_{dif} + k_-^{act}} \tag{56}$$

the diffusion of the fragments out of the solvent cage, the cleavage being at equilibrium, as expressed by eq 57.[22]

$$k_+ = K k'_{dif} \qquad k_- = k_{dif} \tag{57}$$

Examples are given in Figure 6. It is remarkable that, for all endergonic reactions, anion radicals and cation radicals of quite different nature fall on the same diffusion-controlled line. Equations 52 and 54 indicate that the smaller the D_P the larger the equilibrium distance, and the larger the internal reorganization the slower the electron-transfer kinetics. Conversely, when D_P is close to D, the expression of the internal reorganization energy, λ_i, is, as shown below (eqs 58−60), which is the same as in the parabolic Marcus model.[13a]

$$\lambda_i = (\sqrt{D} - \sqrt{D_P})^2 \cong \frac{(D - D_P)^2}{4D} \tag{58}$$

$$\Delta y = y_P - y_R = \frac{1}{\beta} \ln\left(\frac{\sqrt{D}}{\sqrt{D_P}}\right) \cong \frac{(D - D_P)}{2\beta D} \tag{59}$$

$$\lambda_i = D\beta^2 \Delta y^2 = \frac{f \Delta y^2}{2} \tag{60}$$

where f is the force constant for stretching the R−X bond.

There is thus an apparent continuity between the kinetics of an electron transfer leading to a stable product and a dissociative electron transfer. The reason for this continuity is the use of a Morse curve to model the stretching of a bond in a stable product in the first case and the use of a Morse curve also to approximately model a weak charge−dipole interaction in the second case. Under these conditions, the passage from a stepwise to a concerted mechanism is progressive, simply depending upon the nature and magnitude of the interaction between the fragments according whether they are relevant to a true bond or are of the charge dipole type.

Finally we may note that interactions between caged fragments may also influence the dynamics of the heterolytic cleavage of ion radicals in a similar manner, insofar as such reactions may be considered as intramolecular dissociative electron transfers. Simple adaptation of the above treatments will provide the governing equations.

Conclusions

A proper description of the competition between stepwise and concerted pathways in thermal electron transfer/bond breaking reactions requires the introduction of three different reactions coordinates for the three steps involved: dissociative electron transfer, outersphere electron transfer, and bond cleavage. For each of these reactions, a reaction coordinate may be defined by combination of the bond stretching and solvent reorganization coordinate appropriate for each of them. A three-dimensional representation using the three reaction coordinates may then be used to follow the competition between the stepwise and concerted pathways upon changing the thermodynamic and activation parameters.

Application of the same type of analysis to photoinduced electron-transfer/bond-breaking reactions allows the derivation of expressions for the quantum yield for the stepwise mechanism that can be compared to the expressions recently derived for the concerted case. Two different expression are derived for an initial electron transfer in the normal and inverted regions, respectively. In the latter case, which corresponds to a rather common situation, the quantum yield may well approach unity and is not necessarily smaller than the quantum yields for concerted mechanisms.

Interaction between the fragments formed upon dissociative electron transfer may persist, although weakened, when going from the gas phase to a polar solvent. Even though weak, they may have a quite significant influence on the dynamics of dissociative electron transfer. Extension of the Morse curve model allows the derivation of tractable equations depicting the influence of such interactions on heterogeneous and homogeneous reaction dynamics.

References and Notes

(1) (a) For reviews see refs 1b−h. (b) Hush, N. S. *J. Electroanal. Chem.* **1999**, *470*, 170. (c) Maletin, Y. A.; Cannon, R. D. *Theor. Exp. Chem.* **1998**, *34*, 7. (d) Lund, H.; Daasbjerg, K.; Lund, T.; Occhialini, D.; Pedersen, S. U. *Acta Chem. Scand.* **1997**, *51*, 135. (e) Lund, H.; Daasbjerg, K.; Lund, T.; Pedersen, S. U. *Acc. Chem. Res.* **1995**, *28*, 313. (f) Savéant, J.-M. Dissociative Electron Transfer. In *Advances in Electron Transfer Chemistry*; Mariano, P. S., Ed.; JAI Press: New York, 1994; Vol. 4, pp 53−116. (g) Savéant, J.-M. *Acc. Chem. Res.* **1993**, *26*, 455. (h) Savéant, J.-M. Single Electron Transfer and Nucleophilic Substitution. In *Advances in Physical Organic Chemistry*; Bethel, D., Ed.; Academic Press: New York, 1990; Vol. 26, pp 1−130.

(2) (a) Saeva, F. D. *Top. Curr. Chem.* **1990**, *156*, 61. (b) Saeva, F. D. Intramolecular Photochemical Electron Transfer (PET)−Induced Bond Cleavage Reactions in some Sulfonium Salts Derivatives. In *Advances in Electron Transfer Chemistry*; Mariano, P. S., Ed.; JAI Press: New York, 1994; Vol. 4, pp 1−25. (c) Gaillard, E. R.; Whitten, D. G. *Acc. Chem. Res.* **1996**, *29*, 292.

(3) (a) Andrieux, C. P.; LeGorande, A.; Savéant, J.-M. *J. Am. Chem. Soc.* **1992**, *114*, 6892. (b) Andrieux, C. P.; Differding, E.; Robert, M.; Savéant, J.-M. *J. Am. Chem. Soc.* **1993**, *115*, 6592. (c) Andrieux, C. P.; Robert, M.; Saeva, F. D.; Savéant, J.-M. *J. Am. Chem. Soc.* **1994**, *116*, 7864. (d) Andrieux, C. P.; Tallec, A; Tardivel, R.; Savéant, J.-M.; Tardy, C. *J. Am. Chem. Soc.* **1997**, *119*, 2420.

(4) (a) Andrieux, C. P.; Savéant, J.-M. *J. Electroanal. Chem.* **1986**, *205*, 43. (b) Antonello, S.; Maran, F. *J. Am. Chem. Soc.* **1997**, *119*, 12595. (c) Pause, L.; Robert, M.; Savéant, J.-M. *J. Am. Chem. Soc.* **1999**, *121*, 7158. (d) Antonello, S.; Maran, F. *J. Am. Chem. Soc.* **1999**, *121*, 9668.

(5) (a) Arnold, B. R.; Scaiano, J. C.; McGimpsey, W. G. *J. Am. Chem. Soc.* **1992**, *114*, 9978. (b) Chen, L.; Farahat, M. S.; Gaillard, E. R.; Gan, H.; Farid, S.; Whitten, D. G. *J. Am. Chem. Soc.* **1995**, *117*, 6398. (c) Chen, L.; Farahat, M. S.; Gaillard, E. R.; Farid, S.; Whitten, D. G. *J. Photochem. Photobiol., A* **1996**, *95*, 21. (d) Wang, X.; Saeva, F. D.; Kampmeier, J. A. *J. Am. Chem. Soc.* **1999**, *121*, 4364.

(6) Robert, M.; Savéant, J.-M. *J. Am. Chem. Soc.* **2000**, *122*, 514.

(7) Wentworth, W. E.; George, R.; Keith, H. *J. Chem. Phys.* **1969**, *51*, 1791.

(8) Marcus, R. A. *Acta Chem. Scand.* **1998**, *52*, 858.

(9) Benassi, R.; Bernardi, F.; Bottoni, A.; Robb, M. A.; Taddei, F. *Chem. Phys. Lett.* **1989**, *161*, 79.

(10) Tada, T.; Yoshimura, R. *J. Am. Chem. Soc.* **1992**, *114*, 1593.

(11) Bertran, J.; Gallardo, I.; Moreno, M.; Savéant, J.-M. *J. Am. Chem. Soc.* **1992**, *114*, 9576.

(12) (a) Savéant, J.-M. *J. Am. Chem. Soc.* **1987**, *109*, 6788. (b) Savéant, J.-M. *J. Am. Chem. Soc.* **1992**, *114*, 10595.

(13) (a) Marcus, R. A. *J. Chem. Phys.* **1965**, *43*, 679. (b) Marcus, R. A. *J. Phys. Chem. A* **1997**, *101*, 4072. (c) Andrieux, C. P.; Savéant, J.-M.; Tardy, C.; Savéant, J.-M. *J. Am. Chem. Soc.* **1997**, *119*, 11546.

(14) Savéant, J.-M. *J. Phys. Chem.* **1994**, *98*, 3716.

(15) (a) Gould, I. R.; Ege, D.; Moser, J. E.; Farid, S. *J. Am. Chem. Soc.* **1990**, *112*, 4290. (b) Gould, I. R.; Young, R. H.; Moody, R. E.; Farid, S. *J. Phys. Chem.* **1991**, *95*, 2068. (c) Gould, I. R.; Farid, S. *Acc. Chem. Res.* **1996**, *29*, 522. (d) Note, however, that the quantum yields in the work quoted, expressed as $\Phi = k_{sp}/(k_{sp} + k_{-act})$ with our notations, correspond to the formation of the free ion radicals before they have time to react on the solvent or other species present in the solution and before they have time to diffuse back toward one another and undergo back electron transfer. The quantum yields under discussion here correspond to the final formation of $X^{\mp}$ in continuous irradiation experiments.

(16) (a) Landau, L. *Phys. Z. Sowjetunion* **1932**, *2*, 46. (b) Zener, C. *Proc. R. Soc. London, Ser. A* **1932**, *137*, 696. (c) Hush, N. S. *Electrochim. Acta* **1968**, *13*, 1005. (d) Newton, M. D.; Sutin, N. *Annu. Rev. Phys. Chem.* **1984**, *35*, 437. (e) Brunschwig, B. S.; Logan, J.; Newton, M. D.; Sutin, N. *J. Am. Chem. Soc.* **1980**, *102*, 5798.

(17) Pause, L.; Robert, M.; Savéant, J.-M. *J. Am. Chem. Soc.*, in press.

(18) A similar conclusion has recently been reached[8] in the treatment of gas phase electron attachment to aliphatic halides using a slightly different model.

(19) (a) Clark, K. B.; Wayner D. D. M. *J. Am. Chem. Soc.* **1991**, *113*, 9363. (b) Laarhoven, L. J. J.; Born, J. G. P.; Arends, I. W.; Mulder, P. *J. Chem. Soc., Perkin Trans. 2* **1997**, 2307. (c) Pratt, D. A.; Wright, J. S.; Ingold, K. U. *J. Am. Chem. Soc.* **1999**, *121*, 4877. (d) Dorrestijn, E.; Hemmink, S.; Hultsmaan, G.; Monnier, L.; Van Scheppingen, W.; Mulder, P. *Eur. J. Org. Chem.* **1999**, *607*, 7.

(20) (a) Christensen, T. B.; Daasbjerg, K. *Acta Chem. Scand.* **1997**, *51*, 317. (b) Daasbjerg, K.; Jensen, H.; Benassi, R.; Taddei, F.; Antonello, S.; Gennaro, A.; Maran, F. *J. Am. Chem. Soc.* **1999**, *121*, 1750.

(21) (a) Counter examples can be found in the electrochemical reduction of perbenzoates,[4d] where the observation of a transition between a concerted and a stepwise mechanism fits with an exothermic cleavage of the anion radicals. (b) The condition to be fulfilled is that the relaxation from $(X^{\bullet})^{\mp} \leftrightarrow X^{\mp}$ [14] does not require much energy. This condition seems easier to achieve with homolytically cleaving ion radicals rather than with heterolytically cleaving ion radicals, in which cleavage may be viewed as an intramolecular dissociative electron transfer.[14]

(22) Anne, A.; Fraoua, S.; Moiroux, J.; Savéant, J.-M. *J. Am. Chem. Soc*. **1996**, *118*, 3938.

(23) (a) Maslak, P.; Asel, S. L. *J. Am. Chem. Soc.* **1988**, *110*, 8260. (b) Maslak, P.; Chapmann, W. H. *J. Chem. Soc., Chem. Commun*. **1989**, *110*, 1810. (c) Maslak, P.; Chapmann, W. H. *J. Org. Chem*. **1990**, *55*, 6334. (d) Maslak, P.; Chapmann, W. H. *Tetrahedron* **1990**, *46*, 2715. (e) Maslak, P.; Narvaez, J. N. *Angew. Chem., Int. Ed. Engl.* **1990**, *29*, 283. (f) Maslak, P.; Vallombroso, T. M.; Chapmann, W. H.; Narvaez, J. N. *Angew. Chem., Int. Ed. Engl*. **1994**, *33*, 73. (g) Maslak, P.; Chapmann, W. H.; Vallombroso, T. M. *J. Am. Chem. Soc*. **1995**, *117*, 12373. (h) Maslak, P.; Narvaez, J. N.; Vallombroso, T. M.; Watson, B. A. *J. Am. Chem. Soc*. **1995**, *117*, 12380.